Chemical Engineering Journal 445 (2022) 136807

Contents lists available at ScienceDirect

Chemical Engineering Journal

journal homepage: www.elsevier.com/locate/cej

Unraveling the mechanisms of carbon nanotube growth by chemical vapor deposition

Georgios P. Gakis, Stefania Termine, Aikaterini-Flora A. Trompeta, Ioannis G. Aviziotis, Costas A. Charitidis *

Research Lab of Advanced, Composite, Nano-Materials and Nanotechnology, Materials Science and Engineering Department, School of Chemical Engineering, National Technical University of Athens, 9 Heroon Polytechneiou Street, Zografos, Athens 15780, Greece

A R T I C L E I N F O

Keywords:
CVD of CNTs
Macroscopic model
Growth mechanism
Competitive phenomena
Carbon diffusion
Catalyst lifetime

A B S T R A C T

The mechanisms of carbon nanotube (CNT) growth by chemical vapor deposition of acetylene on Fe/SiO_2:Al_2O_3 (zeolite Y) catalyst are unraveled through a combined computational and experimental study. CNTs are synthesized in a horizontal reactor under atmospheric pressure within the temperature range 650 °C–850 °C and characterized by SEM, TEM and Raman spectroscopy. A macroscopic computational fluid dynamics (CFD) model accounting for fluid flow, heat transfer and species transport is developed for the process, incorporating also kinetic expressions for acetylene surface decomposition, acetylene gas-phase reactions, carbon diffusion through the bulk of the catalyst, carbon surface accumulation on the catalyst surface and eventually, CNTs growth. The experimental behavior of the CNTs growth can be accurately described by the proposed macroscopic model. Most importantly, theoretical predictions suggest that there are two distinct temperature regimes for CNTs formation: at the low temperature regime, the process is dominated by the competition between carbon diffusion through the catalyst and carbon impurity layer formation on the catalyst surface, while at higher temperature, the gas-phase reactions of acetylene prevails, releasing byproducts that deposit on the catalyst surface in the form of carbon impurities. Finally, using the developed computational approach, the catalyst lifetime, which is directly affected by these mechanisms, is correlated with the CNTs growth process.

1. Introduction

During the last two decades, an explosion in the use of synthetic and composite nanomaterials has been noticed, stimulated by novel properties stemming from their crystal structure and nano-dimensions. Being in the center of this burst, carbon nanotubes (CNTs) have attracted enormous scientific interest due to their fascinating properties rendering them ideal candidates for industrial applications [1]. Their electronic properties, the high thermal and electrical conductivity as well as the high aspect-ratio and tensile strength are only few of CNTs properties which have attracted scientific interest to explore new routes in several fields and applications ranging from batteries [2], sensors [3] and energy storage [4–6] to electro-catalysis [7,8], environmental engineering [9] and biotechnology [10]. The most commonly applied methods for CNTs synthesis are laser ablation, arc discharge and chemical vapor deposition (CVD) [11]. Amongst them, CVD and in particular, catalytic CVD (CCVD), provides an attractive method for CNTs growth due to its low cost and controllable production of CNTs which in turn, offers the potential for the upscale of the overall process.

However, the control of the process and consequently, its considerate upscale, passes through the understanding of the complex mechanisms occurring during CVD, which combine transport phenomena with chemistry mechanisms and reaction kinetics [12–14]. Therefore, it is crucial to understand those phenomena and mechanisms resulting in the CNTs growth.

An important number of scientific works have been carried out to this direction. Grujicic et al., developed a computational model taking into account a detailed scheme for methane gas-phase and surface reactions (34 and 19, respectively) resulting in the CNTs growth and the deposition of amorphous carbon [15,16]. The reactor model managed to reproduce experimental results in a reasonably good agreement and it provided information for the efficiency of the applied cobalt, nickel and iron catalysts. Puretzky et al., described only the surface reactions of the acetylene precursor in their modeling [17], while Lysaght and Chiu

* Corresponding author.
E-mail address: charitidis@chemeng.ntua.gr (C.A. Charitidis).

https://doi.org/10.1016/j.cej.2022.136807
Received 20 December 2021; Received in revised form 29 April 2022; Accepted 2 May 2022
Available online 6 May 2022

incorporated gas-phase reactions of acetylene [18]. However, in the latter case the gas-phase reactions were adopted from the computational model of CNTs growth from methane.

More recently, Kwok et al., developed a model to study the temperature and time dependence of single-walled CNT (SWCNT) growth, where only surface processes for the ethanol precursor were taken into account [19]. Still, theoretical predictions accurately reproduced the experimental behavior although overestimating the ratio of SWCNTs to amorphous carbon at high temperature. In their work, Ma et al., inspired from the research of Colket et al. [20], described a detailed scheme for acetylene gas-phase pyrolysis, comprising 53 reactions [21]. Based on their simulations, they suggested that the rate-limiting step is a dependent on the catalyst particle size; however, surface processes such as amorphous carbon formation or catalyst deactivation were neglected. Voelskow et al., developed kinetic equations for the description of CNTs growth and catalyst deactivation based on the experimentally measured gas composition as a function of time and they proposed a first-order CNTs synthesis rate and a second-order catalyst deactivation rate [22].

From the discussion so far, it can be generally deduced that the CNTs growth process during CVD involves the following steps: (i) surface decomposition of the precursor on catalyst, followed by the formation of catalyst-C bonds, (ii) diffusion of carbon through the catalyst towards CNTs formation, which is competitive to the carbon accumulation on the surface of the catalyst towards amorphous carbon formation and (iii) gas-phase reactions of the precursor molecule, which can affect the overall growth process. However, there is no modeling of the process combining the effects from the distinguished mechanisms. As a result, there are still open issues for the CNTs growth process such as the determination of the dominating mechanism as a function of the temperature and the dependence of the growth on the reaction-limited or the transport-limited regime. Moreover, there is no modelling process so far taking into consideration what happens to the catalyst during the CVD process, when the catalyst deactivates and which are the mechanisms resulting in this catalyst deactivation. The answers to those questions are of vital importance since they can lead to a considerate, knowledge-based process upscale where the various operating parameters will be chosen *a priory* to have an optimum result concerning both the CNTs and the catalyst.

The present work aims at investigating and decouple the effect of individual mechanisms in the overall CNTs growth process by CCVD of acetylene. This will allow to illustrate the growth-limiting steps as a function of the temperature and to provide a more general and reliable model capable of describing accurately the CNTs production process. The study is based on the comparison of theoretical predictions from the developed computational model incorporating both surface and gas-phase reactions with corresponding experimental measurements. This combined computational and experimental study not only provides valuable insights on the prevailing mechanisms during the CVD of CNTs and discuss their individual effects on the overall growth process but also allows, for the first time for such a computational model, deriving information for the catalyst lifetime during the process.

2. Materials and methods

2.1. Experimental

Growth experiments of CNTs are conducted in a horizontal, tubular, hot wall, quartz CVD reactor which has been described in detail elsewhere [23]. The reactor is placed in a three-zone cylindrical furnace, with a total length of 45 cm. Synthesis of CNTs was conducted using the supported catalyst approach for which the iron catalyst particles are supported on zeolite Y (SiO_2:Al_2O_3, Alfa Aesar, particle size 1 μm; specific surface area 975 m^2/g), at 20 wt%, as prepared with the co-precipitation method [23].

The Fe/SiO_2:Al_2O_3 catalyst particles (~0.2 g) are dispersed homogeneously on a 9.7 × 3.4 × 0.1 cm^3 silicon coupon prior their introduction in the middle of the heating zone of the CVD reactor. Pure Nitrogen (N_2 – 99.998%) is fed in the CVD reactor and the flow rate is measured through electronic mass flow meters (Omega, FMAA2000-Series). Purging is applied for 30 min prior heating the reactor, in order to remove residual air (mainly oxygen), which can cause combustion and oxidation. Afterwards, the reactor is heated to the targeted temperature of each deposition experiment under continuous N_2 flow and atmospheric pressure. The studied temperature range is within 650 °C–850 °C. Once the deposition temperature is reached, a mixture of N_2 (240 sccm) and acetylene (60 sccm, 99.9% Evripos Gases) is fed in the reactor. The CNTs growth time is 4 h in all experiments. For the investigation of the dependence of the growth on the reaction time, different deposition duration is applied. When the experiment is completed, the furnace is turned-off and the reactor is left to cool down to room temperature under continuous N_2 flow. The received product shows a sponge-like form at the end of the CVD experiment.

For CNTs characterization, scanning electron microscopy (SEM – FEI Nova NanoSEM 230) is used to study their morphology and transition electron microscopy (High Resolution TEM JEOL 2011, 200 kV, with a point resolution of 0.194) to determine characteristics such as external and internal diameter, number and thickness of the walls and distance between the walls. Additionally, Raman spectroscopy (Renishaw In-via Raman Spectrometer) is applied to observe the characteristic CNTs modes as well as thermogravimetric analysis (TGA – Netzsch 409 EP) under oxidative atmosphere (atmospheric flow – 100 ml/min, 5 °C/min, temperature range: 25–900 °C) is used for the quantification of amorphous carbon, carbon impurities, and the deposited CNTs.

2.2. Computational modeling

2.2.1. Governing equations and model assumptions

The gas mixture flow inside the CVD reactor is modeled using the continuum medium hypothesis. This hypothesis is validated by calculating the Knudsen number, defined as:

$$\mathrm{Kn} = \lambda / L \tag{1}$$

$$\lambda = \frac{k_B T}{\sqrt{2}\pi d^2 P} \tag{2}$$

where λ is the mean free path of the gas particle and L is the characteristic length, taken equal to the reactor tube diameter in the present work. k_B is the Boltzmann constant, T is the gas-phase temperature, d is the gas species (N_2) particle diameter, and P is the process pressure. For the present study, the continuum medium hypothesis is valid since the calculated $\mathrm{Kn}_{max} = 9.54 \cdot 10^{-6} \ll 0.1$ [24].

The flow inside the CVD reactor tube can be assumed to be laminar, as indicated by the Reynolds number for fluid flow within a pipe:

$$\frac{Re = \rho \cdot u \cdot D}{\mu} \tag{3}$$

where ρ is the mixture density, u is the gas velocity, D is the tube diameter, and μ is the dynamic viscosity of the gas. In the present study, $\mathrm{Re}_{max} = 11.89$. The low value calculated for the Reynolds number validates the laminar flow assumption. The gas mixture is assumed to behave like an ideal gas.

Based on these assumptions, the governing equations for the description of transport phenomena inside the tubular CVD reactor include the conservation of mass, momentum, and energy, coupled with the conservation of chemical species. These equations have been widely used for the modeling of deposition processes and have been described in detail elsewhere [25,26].

The thermal conductivity, dynamic viscosity, and diffusion coefficients for the chemical species are calculated using the kinetic gas theory (COMSOL Multiphysics Reference Manual). The Lennard-Jones parameters for the species are obtained from the CHEMKIN-PRO data-

base [27]:

$$\mu_i = 2.669 \bullet 10^{-6} \frac{\sqrt{TM_i} \bullet 10^{-3}}{\sigma_i \Omega_D} \quad (4)$$

where μ_i is the dynamic viscosity, σ_i is the Lennard-Jones characteristic diameter and Ω_D is the collision integral for viscosity, defined as a function of the dimensionless temperature as $\Omega_D = f(Tk_B/\varepsilon_i)$, with ε_i/k_B being the Lennard-Jones energy potential.

The binary diffusion coefficient can be given by the following expression:

$$D_{i,j} = 2.695 \bullet 10^{-3} \frac{\sqrt{T^3 (M_i + M_j)/(2 \bullet 10^{-3} M_i M_j)}}{\rho \sigma_i \sigma_j} \bullet f\left(\frac{\varepsilon_k}{k_B}\right) \quad (5)$$

with $\varepsilon_k = \sqrt{\varepsilon_i \varepsilon_j / k_B^2}$, and the thermal conductivity is calculated by eq. (6), derived from the kinetic theory of gases:

$$k_i = 2.669 \bullet 10^{-6} \frac{\sqrt{TM_i} \bullet 10^{-3}}{\sigma_i^2} \bullet \frac{1.15 C_{p,i} + 0.88R}{M_i \Omega_D} \quad (6)$$

where $C_{p,i}$ is the specific heat capacity of species i. Finally, the heat capacity for each species is given as a polynomial function of temperature, following the NASA format [28]:

$$\frac{C_P}{R} = a_1 + a_2 T + a_3 T^2 + a_4 T^3 + a_5 T^4 \quad (7)$$

No-slip condition is imposed on the reactor walls for the gas mixture. The outlet pressure is set to atmospheric, while the inflow rates of the N_2 carrier gas and acetylene are set identical to the experimental inflow rates (240 sccm and 60 sccm, respectively – see Section 2.1). The temperature of the walls within the heating zone is set equal to the corresponding experimental oven temperature, while that of the inlet is equal to 20 °C. The reactor walls outside the heating zone are assumed to exchange heat with the reactor environment with an expression given by the following equation:

$$Q = h \bullet (T - T_{ext}) \quad (8)$$

where h is the heat transfer coefficient, and T_{ext} is the temperature of the reactor environment (20 °C).

The described set of equations is discretized and solved using Comsol Multiphysics® with the finite elements method. A quadratic basis function is selected for the velocity, while a linear basis function set is used for temperature, chemical species and pressure. The computational domain is discretized with a computational mesh provided by the software. The mesh consists of 68,366 tetrahedral elements. The final mesh is selected after a dependence study regarding the effect of the computational mesh on the model solution.

2.2.2. Gas-phase reactions

Acetylene in the gas mixture can undergo gas phase reactions during the CVD of CNTs, once entering the heating zone of the reactor [29]. Ma et al. used a reaction model, inspired from the work of Colket [30], to simulate the acetylene decomposition in a CVD reactor similar to the one of this work [21]. The gas phase reaction model proposed by the authors consists of 20 gas species and 53 gas phase reactions. The process of acetylene decomposition is initiated by the reaction [21]:

$$C_2H_2 + C_2H_2 \rightarrow C_4H_3 + H \quad (R1)$$

This is also the energetically limiting step of the gas phase reactions, with an activation energy of 2.62 eV. The initial hydrogen atom is released and subsequently reacts with gas-phase hydrocarbons:

$$C_2H_2 + H \rightarrow C_2H_3 \quad (R2)$$

$$C_2H_3 + C_2H_2 \rightarrow C_4H_4 + H \quad (R3)$$

while the reaction chain can continue to form polycyclic aromatic hydrocarbon molecules [21]. These reactions have a lower activation energy, compared to R1 [21]. The polycyclic aromatic hydrocarbons, formed through the gas phase reactions of acetylene, may result in the subsequent formation of soot and carbon impurities [17,31]. Furthermore, the direct dissociation of acetylene is described [21]:

$$C_2H_2 \rightarrow C_2H + H \quad (R4)$$

However, R4 has a high activation energy of 4.64 eV which renders it improbable to occur in the investigated temperature range of the present study and thus, it is not taken into account.

Based on the above discussion, we decided to lump the gas phase mechanism into a single gas phase reaction to save computational time and cost and at the same time retain a consistent description of the gas phase kinetics. The gas phase reaction used in the presented model is given by the following equation:

$$C_2H_2 + C_2H_2 \rightarrow C_4H_4 \quad (R5)$$

C_4H_4 is a pseudo-species representing the hydrocarbons formed during acetylene gas phase reactions, which do not contribute in the formation of CNTs, but in the formation of carbon impurities. The reaction rate for this reaction was assumed to follow first order Arrhenius kinetics, given by the following rate expression:

$$R_{gas} = A_f \bullet e^{\left(\frac{-E_{a,gas}}{RT}\right)} \bullet C_{acet}^2 \quad (9)$$

In eq. (9), C_{acet} is the acetylene gas-phase concentration, A_f is the pre-exponential factor, and $E_{a,gas}$ is the activation energy, which is assumed equal to the activation energy of reaction R(1), as it is the energetically limiting step for subsequent reactions. The gas-phase reaction rate of eq. (9) is imposed as a source term to the acetylene species conservation equation.

2.2.3. Surface chemistry mechanisms

The mechanism for acetylene adsorption, dissociation and CNT formation is summarized and schematically presented in Fig. 1. The CNTs growth can follow either a tip or base growth mode, depending on strength of interaction between the catalyst particles and the substrate or support. Weak interactions lead to tip growth, as the CNT formation "pushes" the catalyst particle towards the tip of the nanotube[32]. Strong substrate/catalyst interactions prevent the particle from leaving the substrate surface, thus leading the catalyst particle remaining at the base of the formed nanotube (base growth) [32]. In base growth, limitations due to gas phase species diffusion through very dense and long nanotube arrays may arise [33]. These limitations do not occur for tip growth, as the catalyst is at the tip of the nanotube, directly exposed the gas phase of the reactor. In the present work, the CNT formation mechanism assumes a tip-growth mode, where CNTs grow with the catalyst particle on the top of the tube. This assumption is verified by our experimental work [34] as well as from literature data [22]. In any case, however, the chemical reactions and mechanisms that take place on the surface of the catalyst are the same for both growth modes.

Acetylene first adsorbs on the catalyst particle, followed by a catalytic dissociation, leaving Fe-C sites on the surface and releasing H_2 in the gas phase, as a byproduct of surface reactions. From then on, surface Fe-C can form stable C–C bonds on the catalyst surface, covering it by a carbon impurity layer and thus, deactivating the catalyst. On the other hand, surface Fe-C can diffuse through the catalyst particle, reaching its edge, and form CNTs. The mechanism presented in Fig. 1 consists of two competitive mechanisms for dissociated acetylene on the surface: (1) formation of a stable carbon impurity layer and (2) diffusion through the catalyst particle followed by CNT formation. Such competitive mechanisms have been used in literature to explain CNT growth, in both experimental [17,35,36] and computational works [17,37].

In the model developed in this work, the adsorption and dissociation

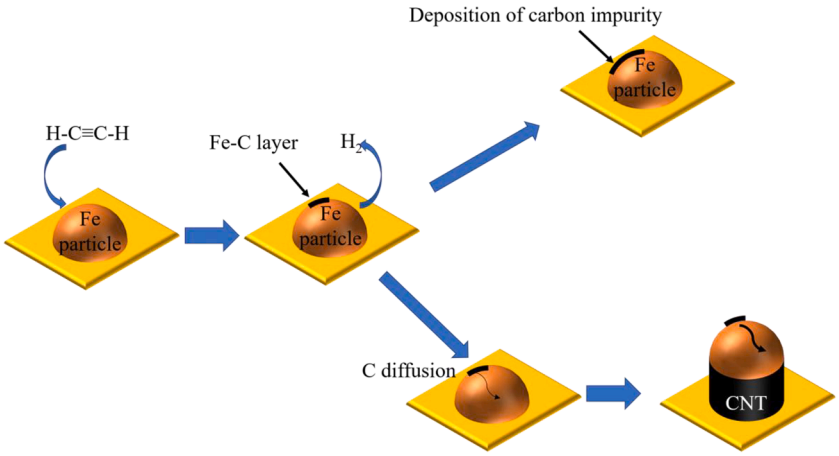

Fig. 1. Schematic representation of the CNT growth mechanism applied in this work.

of the acetylene molecule on the catalyst surface are lumped into a single chemisorption step:

$$R_{ads} = \frac{s \bullet p_{acet}}{\sqrt{2} \bullet \pi \bullet M_{acet} \bullet R \bullet} T \tag{10}$$

where p_{acet} is the acetylene partial pressure, and s is the reactive sticking coefficient:

$$s = s_0 \bullet e^{\left(\frac{-E_{a,acet}}{RT}\right)} \bullet (1 - \theta_c - \theta_{c,im}) \tag{11}$$

In eq. (11), s_0 is the pre-exponential term of the reactive sticking coefficient for a Fe surface fully available for deposition, θ_c is the surface coverage of Fe-C species on the catalyst surface, and $\theta_{c,imp}$ is the surface coverage due to the carbon impurity layer.

Once chemisorbed on the surface, Fe-C can form stable carbon impurities, or diffuse and form CNTs, with a rate calculated from the following expressions, respectively:

$$R_{imp} = k_{imp} \bullet C_c \tag{12}$$

$$R_{CNT} = \frac{D_0 \bullet e^{\left(\frac{-E_{a,diff}}{RT}\right)}}{R_{part}{}^2} \bullet C_c \tag{13}$$

In eq. (12), k_{imp} denotes the rate of impurity formation, while in eq. (13), D_0 stands for the diffusion coefficient of C in the catalyst particle, $E_{a,diff}$ is the activation energy for this diffusion and R_{part} is the catalyst particle radius. The latter expression is used as the main mechanism for CNT formation, as the diffusion through the catalyst particle has been found to be the limiting step for CNT formation [38–40].

Beside the adsorption of acetylene on the free metal catalyst surface, the gaseous pseudo-species, C_4H_4, produced from reaction R(5), can also be adsorbed on the catalyst surface, leading to the production of carbon impurities on the surface:

$$R_{pyr} = \frac{s_{c4h4} \bullet p_{c4h4}}{\sqrt{2} \bullet \pi \bullet M_{c4h4} \bullet R \bullet} T \tag{14}$$

$$s_{c4h4} = s_{0,c4h4} \bullet e^{\left(\frac{-E_{a,c4h4}}{RT}\right)} \bullet (1 - \theta_c - \theta_{c,im}) \tag{15}$$

Finally, both C_2H_2 and the C_4H_4 pseudo-species can contribute to the deposition of carbon films on top of the already deposited carbon impurity layer through a similar mechanism, as in Eqs. (12) and (14).

The surface chemistry model is coupled with the reactor (CFD) model, through the use of a species flux boundary condition (Eqs. (10), 12, 14) for each imposed on the species conservation equation. The parameters and their numerical values used in this work are summarized in Table 1.

3. Results and discussion

3.1. Experimental growth of CNTs by CVD of acetylene

The CNTs deposited by 4 h CVD within the temperature range 650 °C-850 °C are measured in terms of mass. The amorphous carbon and carbon impurities were quantified by TGA[23]. The CNTs mass is obtained by subtracting the catalyst, amorphous carbon and impurities mass from the total measured mass. The resulting CNT mass and the corresponding carbon conversion to CNTs are shown in Fig. 2. Since the CVD duration and hence the total amount of carbon fed to the reactor was the same for all temperatures, the CNT mass and conversion are directly proportional. It is noted here, that with the method described above, the resulting mass presented in Fig. 2 may include structurally defective CNTs and CNT-like carbon nanostructures. However, as the scope of the present study is the investigation of the CNT growth mechanisms, the resulting mass from the above method will henceforth be referred to as CNT mass. This is due to the fact that the defective CNT-like structures are formed through a catalytic process, that includes carbon diffusion through the catalyst and crystalline carbon structure formation, similar to the CNT growth mechanism.

Experimental measurements show a temperature dependence of CNTs growth. At 650 °C, CNTs deposition is lower, with a 27.6% carbon CNT yield. As the process temperature increases, the deposited CNTs mass and yield increases, leading to a maximum of ~ 52.6% carbon CNT yield, at 750 °C. Further increase of the process temperature, however, leads to a decreased CNTs deposition, with the carbon yield equal to 27.2% at 850 °C. This behavior on the CNTs growth as a function of

Table 1
Summary of chemical reaction parameters

	Parameter	Value	Unit
Gas phase reactions	A_f	$1.5 \bullet 10^9$ (fitted)	$\frac{m^3}{mol \bullet s}$
	$E_{a,gas}$	2.62 [21]	eV
Surface reactions	$s_{0,acet}$	0.3 (fitted)	–
	$s_{0,c4h4}$	0.0045 (fitted)	–
	$E_{a,acet}$	0.6 eV[17]	eV
	$E_{a,c4h4}$	0.6 eV (=$E_{a,acet}$)	eV
	E_i (C on C_{imp} layer)	1 (assumed)	eV
	k_{imp}	23 (fitted)	$\frac{1}{s}$
	D_0	0.5 [17,39]	$\frac{cm^2}{s}$
	$E_{a,diff}$	1.5 [17,39]	eV
	R_{part}	5 (experiments)	nm

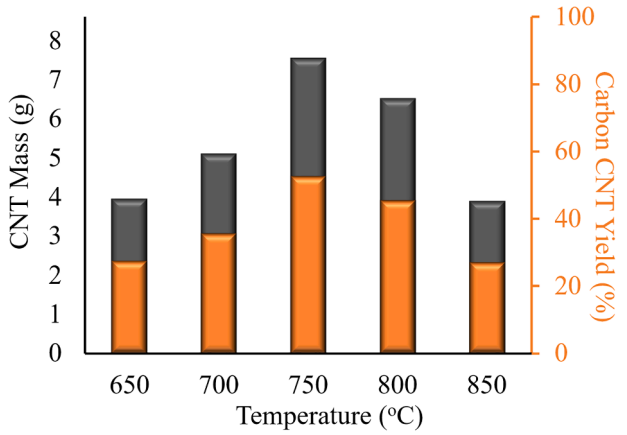

Fig. 2. Measured CNT mass (dark grey column bar, left axis) and derived carbon CNTs yield (orange column bar, right axis) within the temperature range 650 °C–850 °C, after 4 h CVD process.

temperature has been reported also in previous works and it has been explained by catalyst mass loss due to evaporation [17,37,41], changes in the catalyst oxidation state [37] and catalyst deactivation [17]. The detailed discussion of the mechanisms and their effects on the CNTs growth, as well as the identification of the limiting steps of the process, will be discussed in subsection 3.3.

The morphology of the deposited CNTs is studied using SEM and TEM techniques. Fig. 3 shows characteristic micrographs of CNTs produced at 700 °C, 750 °C and 850 °C. The selection of these temperatures is indicative of the behaviour seen in Fig. 2: 700 °C refers to the low-temperature regime of the process, 850 °C to the high-temperature regime, while at 750 °C the optimal carbon CNT yield and I_G/I_D ratio was obtained, as it will be presented in the following sections.

SEM and TEM analyses revealed a clear formation of CNTs at 700 °C and 750 °C. The CNTs length is estimated in the order of several μm, although it is not possible to be accurately measured from SEM, as the CNTs grow in bundles on the catalyst powder. TEM analysis shows MWCNTs formation, with a core diameter of 10 ± 2 nm, following the catalyst particle size applied during the CVD process, justifying our selection for 10 nm diameter catalyst particles within the computational model (see Table 1). The number of walls vary from 10 to 20 for both samples, with a standard interplanar spacing of 3.35 Å between them. On the other hand, at 850 °C, SEM analysis showed that a lower amount of CNTs was formed, again showing the temperature effect on the CNT growth, as in Fig. 2. TEM analysis for this temperature also shows a poor morphology of the synthesized carbon structure, with a significant amount of carbon impurities deposited on the sample.

The quality of the deposited CNTs is investigated by means of Raman spectroscopy to identify the characteristic modes. The Raman spectra of CNTs produced at 700 °C, 750 °C and 850 °C are shown in Fig. 4.

The Raman spectra of Fig. 4 show the characteristic modes for CNTs formation [19]. The G-band, at ~ 1590 cm^{-1} is the tangential mode, corresponding to the in-plane bond stretching mode of the C—C bonds in the hexagonal lattice, typical for the sp^2 carbon materials [42]. The D-band, at ~ 1310 cm^{-1}, corresponds to defects in the crystalline structure of CNTs, and the possible presence of carbon impurities, such as carbon nanoparticles (see also Fig. 3, bottom right), deposited graphitic carbon, or amorphous carbon [19,42]. The G'-band (2D-band), at ~ 2620 cm^{-1} is attributed to a second-order Raman scattering due to a vibrational mode characterized by the breathing of six carbons pertaining to a

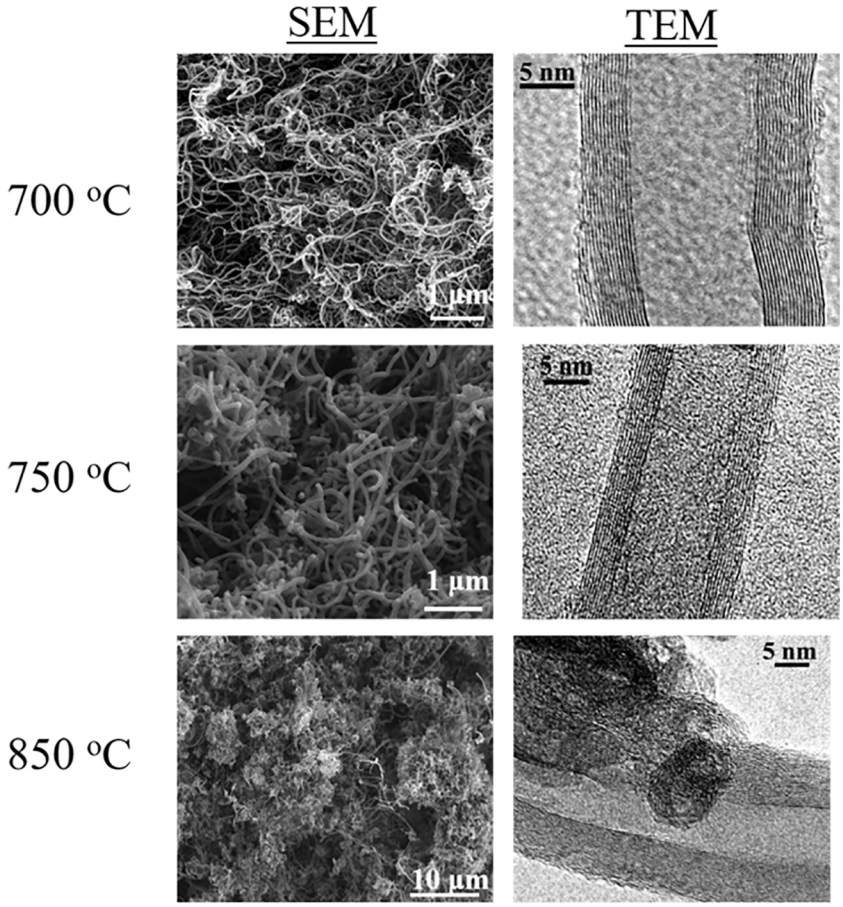

Fig. 3. SEM and TEM micrographs for CNTs deposited at 700 °C, 750 °C and 850 °C.

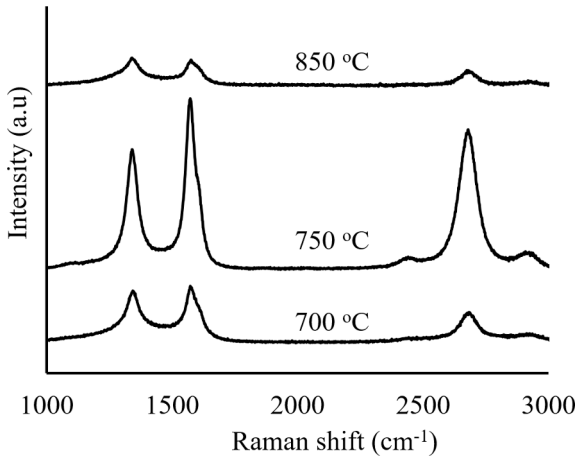

Fig. 4. Raman spectra of deposited CNTs at 700 °C, 750 °C and 850 °C, after 4 h of CVD.

hexagon in the hexagonal lattice of CNTs. Such characteristic modes can be seen in Fig. 4, in the Raman spectra. At 700 °C and 750 °C, sharp and pronounced G and G' modes are observed, showing clearly the formation of CNTs. The additional D modes observed implying the presence of structural defects in the CNTs lattice and of amorphous carbon within the measured sample. As the process temperature increases to 850 °C, the Raman modes become less pronounced and the broadening which is observed especially for the G' mode is attributed to the presence of amorphous carbon in the measured sample [42]. Furthermore, the increased temperature may result to increased carbon impurities deposition, which in turn leads to defected crystal structure, consequently affecting the final properties of the deposited CNTs.

The present work reveals the main mechanisms responsible for the deposition of carbon impurities in the following sections 3.3 and 3.5, where the results of the developed computational model are presented.

3.2. Reactor model: Flow and temperature field

The first step towards the investigation of CNTs deposition by CVD of acetylene is the investigation of the dominant transport phenomena occurring in the CVD reactor. The resulting flow field within the reactor, for a furnace temperature of 750 °C, is shown in Fig. 5**a** (streamlines and velocity vector), on a plane along the flow direction, perpendicular on the catalyst support, for better visualization. In Fig. 5**b**, the gas velocity vector corresponding to the main flow direction is shown at a cross section of the reactor at the furnace entrance.

The resulting flow field in Fig. 5**a** shows gas flow recirculation at the entrance and exit of the heating zone of the CVD reactor. Although the gas enters the reactor with a plug flow regime, due to the rapid heating upon entering the furnace, recirculation occurs, with part of the gas recirculating back, towards the reactor inlet. A similar behavior is observed upon the exit of the gas from the furnace, due to the sharp temperature gradient. This can be seen in Fig. 5**b**, on a reactor cross section, where the gas velocity is plotted. The main gas stream flows on the lower side of the tube (positive velocity), while a part of the gas flows back, towards the inlet, from the upper side of the reactor (negative velocity). This behavior can be explained by the rapid temperature increase upon entering the heating zone, yielding buoyancy effects [43]. The rapid temperature increase leads to a decrease in the gas mixture density, resulting in a density gradient significant enough to trigger gas flow recirculation. This effect is shown in Fig. 6**,** where the temperature field and gas density results are presented.

As it can be observed in Fig. 6**a**, the temperature of the gas-phase increases rapidly once it enters the heating zone of the reactor. This event impacts on the density of the gas (Fig. 6**c**), leading to buoyancy effects and to gas recirculation. The recirculating gas flow stream from the reactor heating zone is heated, and can affect the temperature field close to the reactor inlet (Fig. 6**a**). In turn, this may result in unwanted gas-phase reactions at the vicinity of the reactor heating zone. Furthermore, the species produced from gas-phase reactions under the effect of high temperature within the reactor heating zone, may recirculate back, towards the reactor inlet. In particular, in high temperature, polycyclic aromatic hydrocarbons can be formed in the gas phase. These species may condense on the reactor unheated walls after their recirculation thus, causing equipment damage. Such behavior has been observed experimentally during the CVD of CNTs, as it is illustrated in Fig. 7**a,** where the part of the reactor tube between the inlet and the furnace is shown. Indicative model results for the temperature and the gaseous reaction byproducts partial pressure, for the corresponding part of the CVD reactor, are shown in Fig. 7**b and 7c**, for a furnace temperature of 800 °C.

In Fig. 7**a**, it can be seen that carbon species are deposited on the top part of the reactor walls as a result of gaseous byproducts, while the bottom part shows no carbon species deposition. Furthermore, some of the deposited byproducts appear to condense on the walls. This is consistent with the computational model results of Fig. 7**b and 7c**; higher temperature and gaseous byproduct partial pressure is computed at the top part of the corresponding reactor model, which can lead to

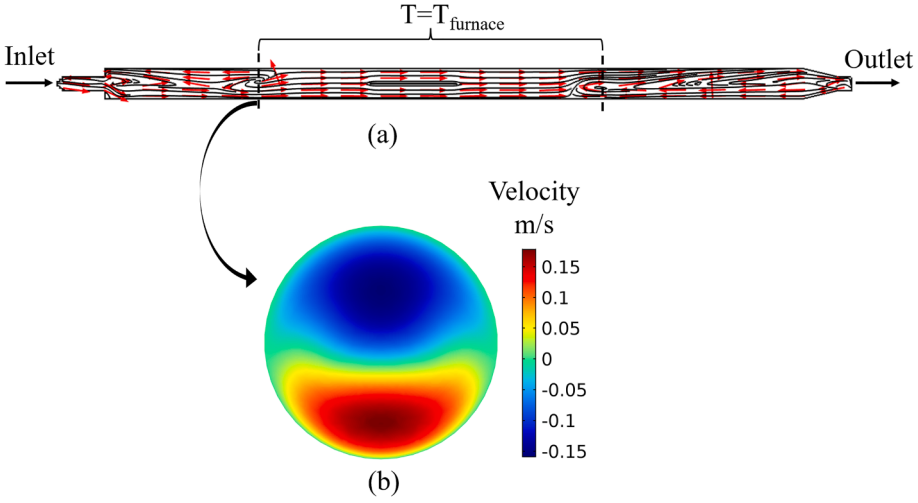

Fig. 5. CFD model results for the flow field within the CVD reactor, for a furnace temperature of 750 °C: (a) streamlines and velocity vector along the reactor, (b) Velocity at a reactor cross section at the entrance of the heating zone.

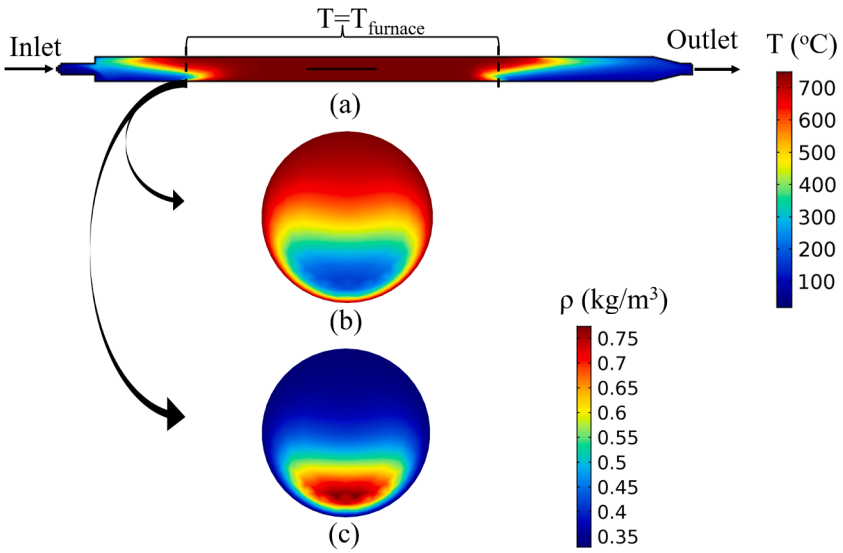

Fig. 6. CFD model results for the temperature field and the gas density within the CVD reactor, for a furnace temperature of 750 °C: (a) Temperature field along the reactor, (b) and (c) Temperature and gas density at a reactor cross section at the entrance of the heating zone, respectively.

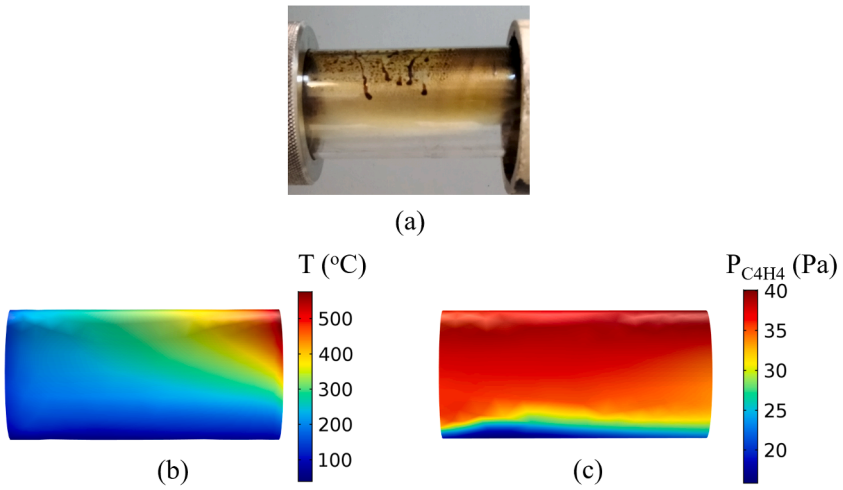

Fig. 7. (a) Image of condensed hydrocarbon byproducts on the reactor walls at the inlet (b) Temperature field and (c) Reaction byproducts partial pressure distribution at the corresponding part of the reactor, as computed from the computational model, for a furnace temperature of 800 °C.

hydrocarbon (e.g. polycyclic) condensation. Although the comparison of this experimental observation with the corresponding theoretical predictions is qualitative, it confirms the validity of the computational model and reveals the dominating transport mechanisms: It is the recirculation of the acetylene precursor heated by the furnace which results in this particular temperature and partial pressure distribution.

Buoyancy effects on the temperature and flow field within tubular CVD reactors for CNT production has been also reported in the literature [43]. However, the detailed impact of buoyancy on the temperature and velocity field, as well as on the CVD equipment due to unwanted gas phase species are presented in this work for the first time, since it has not been linked to these phenomena so far.

The discussion for the temperature and flow field distribution implies that CVD process parameters should be carefully adjusted to optimize the gas flows in terms of minimizing recirculation within the reactor. The control of the flow field, through the modeling of transport phenomena for different process parameters, can eventually assist towards a knowledge-based process control and upscale. A detailed analysis of the process parameter effects on recirculation phenomena and the impact on the gas phase species distribution will be the subject of a future work, since the scope of the present work is to investigate the chemistry mechanisms leading to the formation of CNTs. Yet, before proceeding to this investigation, the effect of transport phenomena in the process for the applied specific conditions should be examined.

3.3. *Chemistry model: CNTs growth mechanism*

The first step towards the CNT growth mechanism investigation is the study of the kinetics of the deposition process. This is done by a combined computational and experimental study to validate the theoretical predictions with respect to the experimental measurements. CNTs were deposited in the temperature range 650 °C–850 °C for different process duration, and the CNT mass for each sample was measured. For the development of the computational model incorporating the chemical reaction mechanisms, the deposition temperature of 700 °C was selected. The choice is based on the fact that at this low temperature, surface reactions are expected to dominate the process and any gas-phase reactions to have less significant effect. The model predictions for the produced CNTs mass and the catalyst surface coverage as a function of time are presented in Fig. 8, along with the corresponding

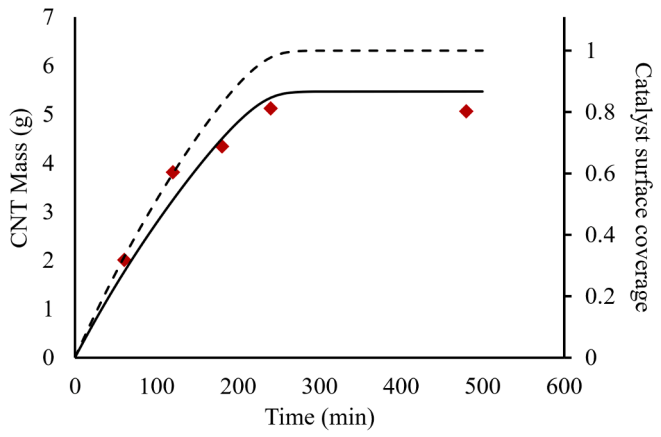

Fig. 8. CNT mass deposition (continuous line, left axis) and catalyst coverage (dashed line, right axis) as a function of time used to conduct CVD at 700 °C, as predicted by the computational model. Experimental measurements for the CNT mass (red squares, left axis) are also shown for comparison.

experimental measurements for the mass of the synthesized CNTs.

Fig. 8 shows an excellent agreement between model predictions and the experimentally measured CNTs mass. The results show an increasing CNTs mass with time, up to the point where saturation of the catalyst surface occurs. The saturation is observed after ~ 4 h under the reactive atmosphere of the experimental procedure. Further increase of process time does not have any effect on the deposited CNTs mass. The ~ 4 h mark corresponds to the time required to cover the whole catalyst surface with a complete carbon impurity layer thus, rendering the catalyst not available for further deposition.

The excellent agreement between theoretical predictions and experimental results allows further investigation of the mechanisms of CNTs growth using the developed computational model. The output from the computational simulations shows that at 700 °C, the acetylene gas phase reaction (reaction R(5)) is not significant. Therefore, the catalyst deactivation is dictated by the competition between carbon diffusion through the catalyst particles (eq. (12)) and the formation of stable carbon species on the catalyst surface (eq. (13)). This mechanism for the catalyst lifetime and deactivation has been also proposed in the literature [17]. Fig. 9 shows the deactivation of the catalyst in terms of catalyst coverage by the carbon impurity layer on the entire catalyst surface. The catalyst surface is treated macroscopically as a whole, rather than the surface of each individual catalyst particle.

Fig. 9 shows that the catalyst surface at the front edge of the silicon wafer where the catalyst is placed (close to the entrance of the heating zone) is deactivated more rapidly from carbon impurities. The catalyst is gradually deactivated in the direction of the gas flow stream, until it is

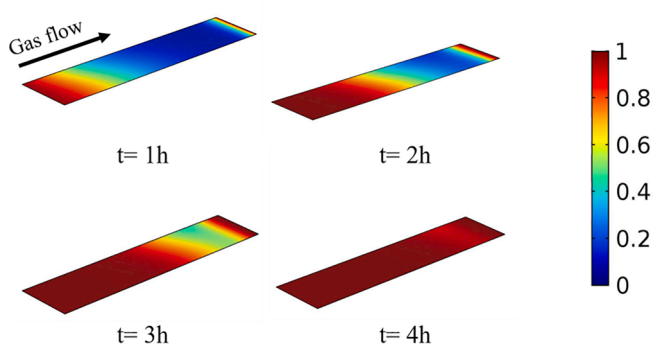

Fig. 9. Catalyst coverage by the carbon impurity layer for 1-hour steps during the CVD of CNTs, at 700 °C. The surface of the catalyst is investigated macroscopically as an ensemble and not as individual catalyst particles.

almost fully covered by carbon after 4 h on stream during the CVD process. It is noted that the back edge of the wafer (close to the exit from the heating zone) is deactivated more rapidly than the center. This can be attributed to the reactants diffusion from the gas stream which flows at underneath the wafer (see Fig. 5), where no catalyst is present: The unreacted gas-phase species may diffuse on the top part of the wafer and undergo surface reactions catalyzed by the catalyst particles at the back edge of the wafer.

For the investigation and illustration of the dominating mechanisms of the CNTs growth, the process is examined computationally in the temperature range 650 °C–850 °C, i.e., identical to the range used for the experimental procedure. Fig. 10 is the Arrhenius-type plot of the process, which shows the CNTs mass as a function of temperature for both theoretical predictions (solid line) and experimental measurements (red squares) after 4 h process time.

In Fig. 10, a satisfactory agreement between computational predictions and experimental measurements is observed, which gives rise to investigate the dominating mechanisms at different temperature regimes. At the low temperature regime (up to 750 °C), the deposited CNTs mass is low, due to the high energy barrier (1.5 eV) required to be overcome for the carbon diffusion through the catalyst particle, which is assumed to be the energetically limiting step of the process. The catalyst deactivation is dictated by the competition between the carbon diffusion though the catalyst and the formation of a stable carbon surface layer.

As temperature increases, the CNTs mass also increases due to the carbon diffusion through the catalyst particle, which is favored over the formation of carbon impurity layer on the catalyst surface. The good agreement between predictions and experimental measurements shows that the diffusion through the catalyst particle as a limiting step can indeed explain the experimental trend thus, validating the assumptions of the model. It is noted that at this temperature regime, up to 750 °C, the gas phase reactions do not have a significant impact on the catalyst deactivation, due to the high energy barrier required (2.62 eV). Furthermore, the catalyst deactivation is dictated by surface reactions through the formation of carbon impurities on its surface.

For the high-temperature regime, i.e., above 750 °C, it is observed in Fig. 10 that CNTs mass is decreasing. This behavior implies a change of the growth mechanism; if the same mechanism would be the limiting step at higher temperature further increase of the CNTs mass should have been observed in the Arrhenius plot. However, since this is not the case, the effect of gas-phase reactions on the process is investigated. Indeed, the acetylene gas phase reaction in the gas phase, described by R5, produces gas-phase species which contribute to the deposition of carbon impurities on the surface of the catalyst, rendering it deactivated. Thus, in the high-temperature regime the catalyst deactivation is

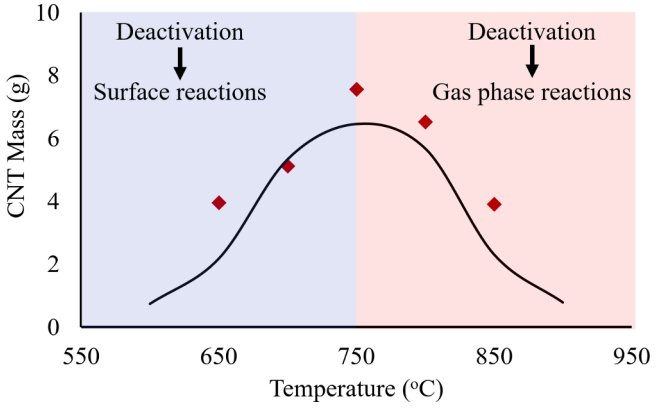

Fig. 10. Arrhenius-type plot of the process showing CNTs mass as a function of temperature, after 4 h of CVD process time. The solid line represents theoretical predictions while red squares experimental measurements. The different color fill denotes the distinct temperature regimes where different mechanisms affect the CNTs growth.

dictated by a second mechanism, namely acetylene gas-phase gas phase reactions, which produces gaseous byproducts that deposit on the catalyst surface in the form of carbon impurities, thus limiting the growth process. It is important to note here that at higher temperatures, sintering of Fe particles may also influence the CNT deposition. The sintering of catalyst particles decreases the active surface of the catalyst and the number of active sites. Indeed, this mechanism could also contribute to the decrease of CNT growth. However, Results of Section 3.1 showed that at higher temperatures, besides the decrease of CNT formation, there is also an increase of carbon impurities deposition. The deposition of these impurities is another hint towards the activation of gas phase reactions at higher temperature, resulting in the deposition of gaseous species in the form of carbon impurities on the catalyst surface. Hence, although sintering may take place at higher temperature, the fact that the model is capable of explaining the behavior of the CNT growth and the higher impurities deposition without taking sintering into account, leads to the deduction that acetylene gas phase reaction byproducts is the major deactivation pathway at the higher temperature regime.

The above analysis and understanding of the mechanisms taking place during the CVD process allows us to distinguish the CVD of CNTs into distinct regimes, characterized by the catalyst deactivation process: a) The surface reaction regime, where the deactivation occurs due to surface reactions and the limiting-step for CNTs growth is carbon diffusion through the catalyst and b) the acetylene gas phase reactions regime, where the growth is limited by the catalyst deactivation due to the gas-phase acetylene reactions yielding the deposition of carbon impurities on the catalyst surface. These two regimes are shown in different color of the plot in Fig. 10.

3.3.1. *Catalyst lifetime*

Beside the temperature effect on the mass of the deposited CNTs, there is also an effect on the catalyst lifetime, i.e. the time required for the catalyst surface saturation and its subsequent deactivation. Using the developed computational model, the catalyst lifetime dependence on the process temperature is investigated. This is the first time that macroscopic computational predictions for the catalyst lifetime are presented to the best of the authors knowledge.

Fig. 11 presents computational predictions for catalyst surface coverage by the carbon impurity layer as a function of time and temperature (Fig. 11**a**) and the resulting catalyst lifetime as a function of process temperature (Fig. 11**b**). Furthermore, Fig. 11**c** shows the correlation of the predicted CNTs mass at the end of the catalyst lifetime with the computationally derived catalyst lifetime.

At low temperature (650 °C), the diffusion of carbon through the catalyst particle is slower, and a larger proportion of carbon atoms from the catalytic surface decomposition of acetylene can produce stable carbon impurities on the catalyst surface. As a result, the catalyst is deactivated and its lifetime is decreasing. This is denoted by the fast surface coverage (less than 100 min) observed in Fig. 11**a**. The temperature increase (up to 750 °C) favors the diffusion of carbon through the catalyst rather than the surface formation of the impurities layer. This leads to the availability of the catalyst active sites, as a previously occupied (from the carbon atom that diffuses) surface site becomes active for adsorption. As a result, the catalyst lifetime is increasing and as a consequence, the formation of more CNTs is favored. The longer

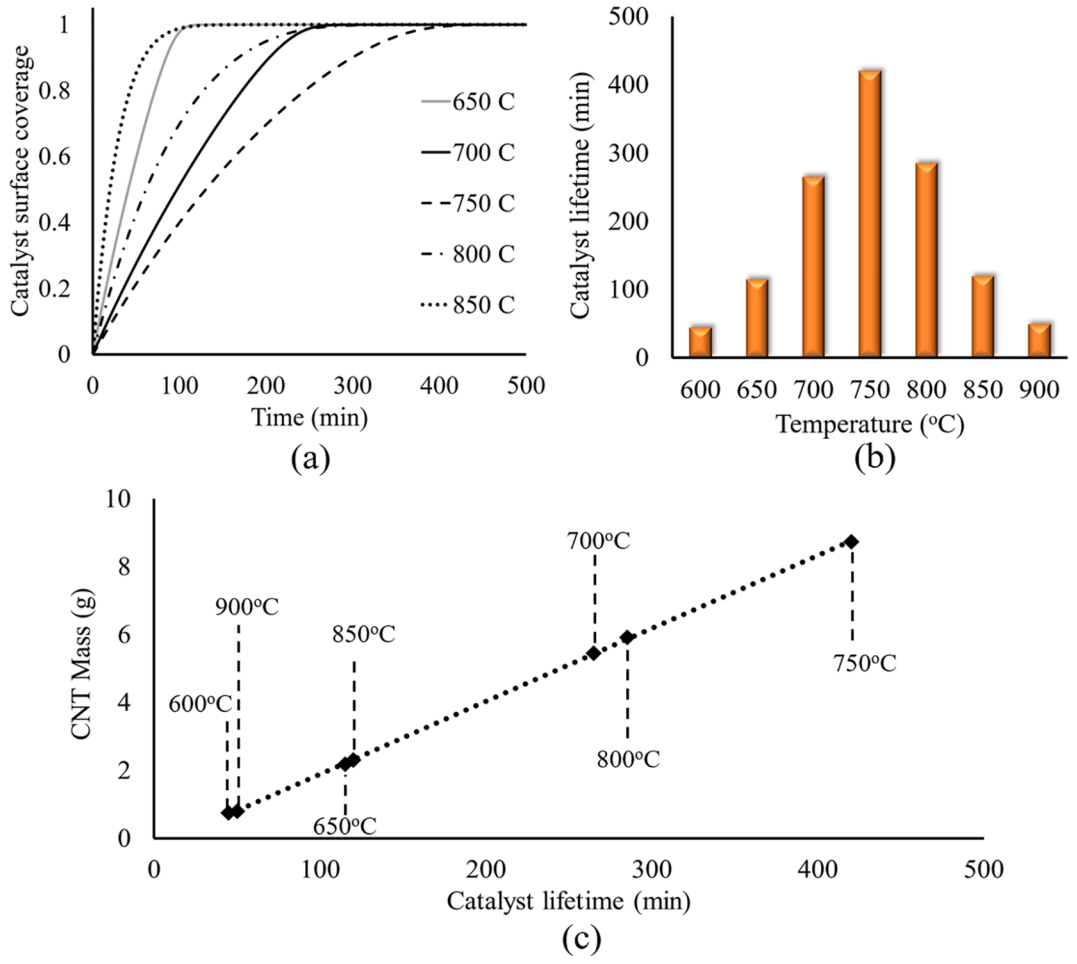

Fig. 11. (a) Catalyst surface coverage by carbon impurities as a function of time and process temperature, (b) Catalyst lifetime as a function of process temperature (c) Model predictions of CNTs mass at the end of the catalyst lifetime as a function of the derived catalyst lifetime.

catalyst lifetime can be seen in Fig. 11**a,** where more time (>200 min) is required for the catalyst surface to be completely covered. Further increase of the temperature (above 750 °C), however, will lead to the gas phase reactions of acetylene, leading to the deposition of carbon impurities on the catalyst surface, thus deactivating the catalyst.

Fig. 11**b** shows the derived catalyst lifetime dependence on the process temperature. The increase of temperature extends the catalyst lifetime from ~ 55 min (600 °C) to ~ 460 min (750 °C) with a simultaneous increase to the CNTs mass. Further increase of the temperature leads to a rapid decrease of the catalyst lifetime, as well as the mass of the produced CNTs. This behavior has been also reported in previous works and it has been attributed to catalyst reduction [44] and catalyst damage [45] at higher temperature. In the present study, the combined computational and experimental approach not only reproduces this behavior, but more importantly, provides an explanation for the catalyst lifetime behavior using the applied physical and chemical mechanisms that is, the formation of carbon impurities formed on the catalyst surface either through surface reactions (T < 750 °C) or through acetylene gas phase reactions byproducts deposition (T > 750 °C).

In Fig. 11**c, a** linear dependence of the CNTs mass on the catalyst lifetime is derived. This dependence reveals the importance of the catalyst lifetime and its deactivation mechanism for the CNT growth: A longer catalyst lifetime results in an increased CNTs deposition. The above-described catalyst deactivation mechanisms for the corresponding process conditions affect the catalyst lifetime significantly and as a consequence the CNTs growth. These aspects should be studied and understood in depth, in order to obtain the optimum process design and conditions, maximizing the lifetime of the catalyst and thus, CNTs production.

3.3.2. *Carbon impurities deposition*

Within the developed computational model, carbon impurities may also form on already deposited carbon layers, beside their deposition on the catalyst particle surface. These species may deposit as amorphous carbon, graphitic layers or other carbon impurities and reduce the purity of the produced CNTs, thus affecting their final properties.

As these species deposit on the already deposited carbon layers, they do not have a major effect on the catalyst surface and on the CNT formation mechanism. The computational model takes the deposition of such species into account, in a qualitative way, due to the lack of experimental measurements for carbon impurities deposition or kinetic parameters describing this process. Computational results for the excess carbon impurities deposition are presented in Fig. 12**a**, where a time dependent evolution of CNTs, carbon impurities and the total mass of carbon produced at 700 °C are shown. It is once again reminded that the impurities deposition on top of already deposited carbon is taken into account in a qualitative way by the present model.

Although deposition of CNTs saturates after a specific time due to catalyst deactivation, the deposition of carbon impurities shows a different behavior. At the initial stages of the process surface carbon is produced, since the catalyst is fully active allowing the surface dissociation of acetylene. The surface carbon can then diffuse or form impurities, as already discussed. Thus, at this stage, the impurity deposition is lower. However, once impurities start to form, they lead to the formation of a stable carbon layer that encapsulates and deactivates the catalyst. On top of this layer, acetylene can only produce impurities, since there is no contact between the gas phase and the catalyst. Therefore, the carbon layer initially formed on the catalyst serves as nucleation center for further carbon deposition in the form of impurities. This is shown by the trend of the carbon impurities mass as a function of time in Fig. 12**a**: Initially, the mass of impurities increases slowly, followed by a transitional period where it increases exponentially with time. Finally, after a certain point which “coincides” with the lifetime of the catalyst, the mass increases linearly with time. It is observed that the total mass of carbon initially increases approximately in the same way as the CNTs mass, until the catalyst is deactivated and the CNTs growth stops. From then on, the total mass increases with the same rate as the carbon impurities. This behavior has been studied experimentally in the literature resulting in the same conclusions [46]. Theoretical predictions of the present work from the developed computational model are in excellent qualitative agreement with those results illustrating the reason behind this trend.

The dependence of carbon impurities deposition on the CVD process temperature are shown in Fig. 12**b**. In theory, for a given time, the deposited impurities should increase with temperature, as expected for a thermally activated process. However, Fig. 12**b** shows a more complex behavior. Initially, between 600 °C and 700 °C, the mass of impurities increases with temperature and then, a decrease is observed up to ~ 750 °C. Above that point, an increase in temperature leads to a sharp increase of the carbon impurities mass.

The behavior observed in the range of 650–800 °C for the processing time shown in Fig. 12**b** is attributed to the fact that the catalyst is not fully deactivated, or the deactivation time is close to the processing time (see also Fig. 11**b**). If the catalyst is not fully covered by the carbon layer, only a part of its surface is available for further deposition of impurities. This is observed in Fig. 12**b**, where, as process time increases, the temperature range in which the mass of impurities decrease occurs becomes narrower. On the other hand, for the 8-hours case, no such

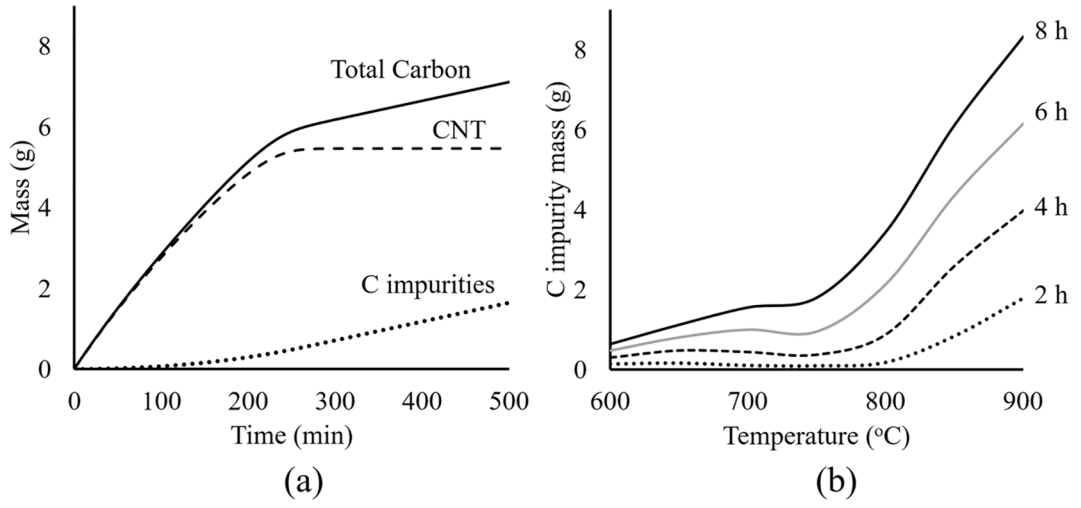

Fig. 12. Model predictions for carbon impurities: (a) CNT, carbon impurities and total carbon mass evolution with CVD process time, at 700 °C, (b) Carbon impurities mass after 2, 4, 6, 8 h, as a function of process temperature.

decrease can be seen between 700 °C and 750 °C but instead a slight increase of the impurities mass is observed. This behavior shows that the catalyst lifetime also has an impact on the total impurities included in the final product of the CVD process. Therefore, to achieve higher CNTs purity, a CVD temperature that extends the catalyst lifetime should be selected combined with process time according to the corresponding lifetime.

The computational model predictions concerning the purity of the deposited CNTs are presented in Fig. 13, where the ratio of the CNTs and impurities mass, after 4 h of CVD is shown. The corresponding I_G/I_D ratio from the Raman characterization of the experimental samples is also presented in Fig. 13, as a qualitative comparison to the theoretical predictions.

Theoretical predictions show that with the increase of temperature, the CNT/impurity ratio increases, up to 750 °C. Further increase of the CVD temperature leads to the decrease of the CNT/impurity ratio. At low temperature, the CNTs/impurities ratio is low due to the slow diffusion of carbon through the catalyst, which leads the carbon species on the catalyst surface to form a carbon impurities surface layer that poisons the catalyst. The catalyst lifetime is shorter, and carbon impurities deposit on the already deposited carbon layer. Increase of temperature favors the diffusion of carbon through the catalyst. Thus, the catalyst lifetime increases, the CNTs formation is promoted and the CNTs/impurities ratio increases. Further increase of the temperature leads to acetylene reactions in the gas phase. The gas phase reactions products yield the deactivation of the catalyst, which results in the deposition of more carbon impurities and lower CNTs/impurities ratio. A similar trend is also seen for the experimental measurements (red squares), for which the intensity ratio I_G/I_D is presented as a function of the temperature. The I_G/I_D ratio has often been used as an indicator of the CNT crystallinity or a measure of either the quality of the produced CNTs or their defected crystal structure, including also not sp^2 carbon [19,42,47]. Although the D-band in the Raman spectra does not correspond only to impurities deposited in the form of carbon species other than sp^2-hybridized, but it also implies the presence of defects in the CNTs lattice, the model can qualitatively reproduce the I_G/I_D ratio behavior as a function of temperature.

It is noted here that the macroscopic computational model developed in this work does not take into account lattice defects and it cannot provide such information. Also, it does not take into account the deposition of carbon impurities on the CNT walls. Finally, kinetic parameters for the deposition of impurities on already deposited carbon, such as activation energy, were assumed in the present model, thus only allowing a qualitative study of the carbon impurities deposition. Nonetheless, although the experimental I_G/I_D and the predicted CNTs/impurities ratio cannot be directly compared to extract quantitative information for the CNTs quality, the qualitative behavior of the predicted CNTs/impurities ratio as a function of temperature allows understanding the key mechanisms for the CNTs purity and its dependence on temperature.

4. Conclusions

The transport phenomena and chemistry mechanisms for the CNTs synthesis by CCVD of acetylene are studied using a macroscopic computational model. Theoretical predictions are in good agreement with corresponding experimental measurements, ensuring the validity of the computational model. The computational investigation illustrated the dominating mechanisms in the applied temperature range of 650 °C–850 °C, which can be divided into two distinct temperature regimes. Valuable information regarding the catalyst lifetime over the CCVD temperature range is provided for the first time in terms of computational modeling, consistent with experimental literature findings.

In the first regime (650 °C–750 °C), the CNTs mass increases with temperature and the process is dominated by the competition between carbon diffusion through the bulk of the catalyst and the formation of a stable carbon layer on the surface of the catalyst causing its deactivation. The increased CNT production is correlated with the catalyst lifetime, which shows a similar behavior with temperature. In this regime, the increase of temperature also yields a higher CNTs/impurities ratio.

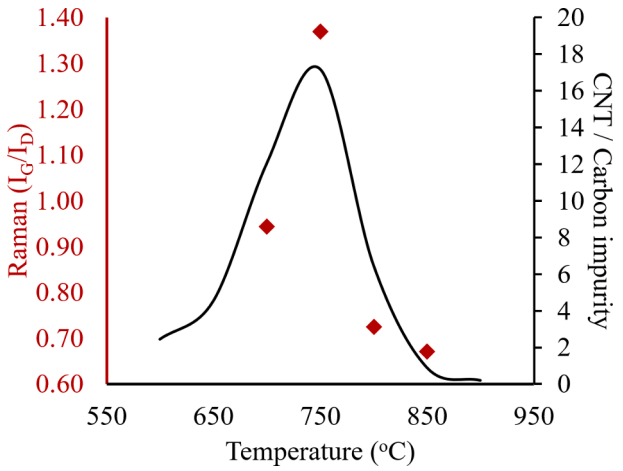

Fig. 13. Model predictions for the ratio of the mass of CNTs and carbon impurities after 4 h of CVD, as a function of temperature (black line). The corresponding I_G/I_D ratio from Raman characterization of experimental samples is also plotted for qualitative comparison (red squares).

In the second regime (above 750 °C), the CNTs mass decreases with temperature and the process is limited by catalyst deactivation via carbon impurities from the acetylene gas phase reactions byproducts. This behavior is also correlated with the decrease of catalyst lifetime at temperatures above 750 °C, due to gas phase impurities deposition. In this regime, the CNTs/carbon impurities ratio also decreases due to the inclusion of carbon impurities in the final product.

The developed computational framework provides a generalized and reliable scheme for the CNTs synthesis by CVD. It can be implemented to conduct simulations for various process parameters, different reactor setups and different hydrocarbon sources. Such studies offer the potential of a knowledge-based process upscale and the possibility of using more environmentally-friendly precursor molecules which have not been studied experimentally in detail.

Declaration of Competing Interest

The authors declare that they have no known competing financial interests or personal relationships that could have appeared to influence the work reported in this paper.

Acknowledgments

This work was funded by the EU H2020 Project ‘Smart by Design and Intelligent by Architecture for turbine blade fan and structural components systems’ (SMARTFAN) under Grant no. 760779. Prof. Thomas Kehagias (Electron Microscopy Laboratory of Physics Department, School of Physics, Aristotle University of Thessaloniki) is acknowledged for the TEM measurements. Prof. Alberto Tagliaferro (Carbon Group, Politecnico di Torino) is acknowledged for the TGA measurements. This work was supported by computational time granted from the Greek Research & Technology Network (GRNET) on the National HPC facility ARIS under project REP3D (pr011037).

References

[1] M.F.L. De Volder, S.H. Tawfick, R.H. Baughman, A.J. Hart, Carbon nanotubes: present and future commercial applications, Science 339 (6119) (2013) 535–539, https://doi.org/10.1126/science.1222453.

[2] S. Zhong, H. Liu, D. Wei, J. Hu, H. Zhang, H. Hou, M. Peng, G. Zhang, H. Duan, Long-aspect-ratio N-rich carbon nanotubes as anode material for sodium and lithium ion batteries, Chem. Eng. J. 395 (2020) 125054.

[3] G. Tian, L. Zhan, J. Deng, H. Liu, J. Li, J. Ma, X. Jin, Q. Ke, C. Huang, Coating of multi-wall carbon nanotubes (MWCNTs) on three-dimensional, bicomponent nonwovens as wearable and high-performance piezoresistive sensors, Chem. Eng. J. 425 (2021) 130682.

[4] X. Lu, L. Zhang, H. Yu, Z. Lu, J. He, J. Zheng, F. Wu, L. Chen, Achieving superior hydrogen storage properties of MgH2 by the effect of TiFe and carbon nanotubes, Chem. Eng. J. 422 (2021) 130101.

[5] S.U. Rather, Preparation, characterization and hydrogen storage studies of carbon nanotubes and their composites: a review, Int. J. Hydrogen Energy 45 (7) (2020) 4653–4672, https://doi.org/10.1016/j.ijhydene.2019.12.055.

[6] P. Bondavalli, D. Pribat, P. Legagneux, M.-B. Martin, L. Hamidouche, L. Qassym, G. Feugnet, A.-F. Trompeta, C.A. Charitidis, Deposition of graphene and related nanomaterials by dynamic spray-gun method: a new route to implement nanomaterials in real applications, JPhys Mater. 2 (3) (2019) 032002.

[7] E. Pajootan, S. Omanovic, S. Coulombe, Controllable dry synthesis of binder-free nanostructured platinum electrocatalysts supported on multi-walled carbon nanotubes and their performance in the oxygen reduction reaction, Chem. Eng. J. 426 (2021) 131706.

[8] Z. Zhao, Z. Zhu, F. Wang, S. Li, X. Bao, L. Zhang, S. Lin, Y. Yang, Bimetallic carbides embedded in heteroatom-doped carbon nanotubes for efficient electrocatalytic hydrogen evolution reaction and high-performance lithium storage, Chem. Eng. J. 415 (2021) 128885.

[9] Y. Wang, C. Pan, W. Chu, A.K. Vipin, L. Sun, Environmental remediation applications of carbon nanotubes and graphene oxide: adsorption and catalysis, Nanomaterials 9 (3) (2019), https://doi.org/10.3390/nano9030439.

[10] V.R. Raphey, T.K. Henna, K.P. Nivitha, P. Mufeedha, C. Sabu, K. Pramod, Advanced biomedical applications of carbon nanotube, Mater. Sci. Eng., C 100 (2019) 616–630, https://doi.org/10.1016/j.msec.2019.03.043.

[11] C.A. Charitidis, P. Georgiou, M.A. Koklioti, A.-F. Trompeta, V. Markakis, Manufacturing nanomaterials: from research to industry, Manuf. Rev. 1 (2014) 11.

[12] I.G. Aviziotis, N. Cheimarios, T. Duguet, C. Vahlas, A.G. Boudouvis, Multiscale modeling and experimental analysis of chemical vapor deposited aluminum films: linking reactor operating conditions with roughness evolution, Chem. Eng. Sci. 155 (2016) 449–458, https://doi.org/10.1016/j.ces.2016.08.039.

[13] G.P. Gakis, E.D. Koronaki, A.G. Boudouvis, Numerical investigation of multiple stationary and time-periodic flow regimes in vertical rotating disc CVD reactors, J. Cryst. Growth 432 (2015) 152–159, https://doi.org/10.1016/j.jcrysgro.2015.09.026.

[14] G.M. Psarellis, I.G. Aviziotis, T. Duguet, C. Vahlas, E.D. Koronaki, A.G. Boudouvis, Investigation of reaction mechanisms in the chemical vapor deposition of al from DMEAA, Chem. Eng. Sci. 177 (2018) 464–470, https://doi.org/10.1016/j.ces.2017.12.006.

[15] M. Grujicic, G. Cao, B. Gersten, Optimization of the chemical vapor deposition process for carbon nanotubes fabrication, Appl. Surf. Sci. 199 (1–4) (2002) 90–106, https://doi.org/10.1016/S0169-4332(02)00892-9.

[16] M. Grujicic, G. Cao, B. Gersten, Reactor length-scale modeling of chemical vapor deposition of carbon nanotubes, J. Mater. Sci. 38 (8) (2003) 1819–1830, https://doi.org/10.1023/A:1023252432202.

[17] A.A. Puretzky, D.B. Geohegan, S. Jesse, I.N. Ivanov, G. Eres, In situ measurements and modeling of carbon nanotube array growth kinetics during chemical vapor deposition, Appl. Phys. A - Mater. 81 (2) (2005) 223–240, https://doi.org/10.1007/s00339-005-3256-7.

[18] A.C. Lysaght, W.K.S. Chiu, Modeling of the carbon nanotube chemical vapor deposition process using methane and acetylene precursor gases, Nanotechnology 19 (16) (2008) 165607.

[19] C.T.M. Kwok, B.J. Reizman, D.E. Agnew, G.S. Sandhu, J. Weistroffer, M.S. Strano, E.G. Seebauer, Temperature and time dependence study of single-walled carbon nanotube growth by catalytic chemical vapor deposition, Carbon 48 (4) (2010) 1279–1288, https://doi.org/10.1016/j.carbon.2009.11.053.

[20] M.B. Colket, D.J. Seery, H.B. Palmer, The pyrolysis of acetylene initiated by acetone, Combust. Flame 75(3–4) 75 (3-4) (1989) 343–366.

[21] H. Ma, L. Pan, Y. Nakayama, Modelling the growth of carbon nanotubes produced by chemical vapor deposition, Carbon 49 (3) (2011) 854–861, https://doi.org/10.1016/j.carbon.2010.10.029.

[22] K. Voelskow, M.J. Becker, W. Xia, M. Muhler, T. Turek, The influence of kinetics, mass transfer and catalyst deactivation on the growth rate of multiwalled carbon nanotubes from ethene on a cobalt-based catalyst, Chem. Eng. J. 244 (2014) 68–74, https://doi.org/10.1016/j.cej.2014.01.024.

[23] A.F. Trompeta, M.A. Koklioti, D.K. Perivoliotis, I. Lynch, C.A. Charitidis, Towards a holistic environmental impact assessment of carbon nanotube growth through chemical vapour deposition, J. Clean. Prod. 129 (2016) 384–394, https://doi.org/10.1016/j.jclepro.2016.04.044.

[24] H. Liao, T.S. Cale, Low-Knudsen-number transport and deposition xGexlayers on Si substrates by rapid thermal chemical vapor deposition, J. Vac. Sci. Technol. A 12 (4) (1994) 1020–1026, https://doi.org/10.1116/1.579278.

[25] G.P. Gakis, H. Vergnes, E. Scheid, C. Vahlas, A.G. Boudouvis, B. Caussat, Detailed investigation of the surface mechanisms and their interplay with transport phenomena in alumina atomic layer deposition from TMA and water, Chem. Eng. Sci. 195 (2019) 399–412, https://doi.org/10.1016/j.ces.2018.09.037.

[26] P.A. Gkinis, I.G. Aviziotis, E.D. Koronaki, G.P. Gakis, A.G. Boudouvis, The effects of flow multiplicity on GaN deposition in a rotating disk CVD reactor, J. Cryst. Growth 458 (2017) 140–148, https://doi.org/10.1016/j.jcrysgro.2016.10.065.

[27] CHEMKIN-PRO, CHEMKIN-PRO 15131, Reaction Design (2013).

[28] B.J. McBride, S. Gordon, M.A. Reno, Coefficients for Calculating Thermodynamic and Transport Properties of Individual Species, NASA Report TM-4513 (1993).

[29] O.A. Rokstad, O.A. Lindvaag, A. Holmen, Acetylene pyrolysis in tubular reactor, Int. J. Chem. Kinet. 46 (2) (2014) 104–115, https://doi.org/10.1002/kin.20830.

[30] M.B. Colket, Kinetic Mechanism for Pyrolysis of Acetylene Near 1000K, Preprints, ACS Division of Fuel Chemistry, 1987, pp. 417–427.

[31] M. Frenklach, S. Taki, M.B. Durgaprasad, R.A. Matula, Soot formation in shock-tube pyrolysis of acetylene, allene, and 1,3-butadiene, Combust. Flame 54 (1–3) (1983) 81–101, https://doi.org/10.1016/0010-2180(83)90024-X.

[32] M.V. Kharlamova, Investigation of growth dynamics of carbon nanotubes, Beilstein J. Nanotechnol. 8 (1) (2017) 826–856, https://doi.org/10.3762/bjnano.8.85.

[33] R. Xiang, Z. Yang, Q. Zhang, G. Luo, W. Qian, F. Wei, M. Kadowaki, E. Einarsson, S. Maruyama, Growth deceleration of vertically aligned carbon nanotube arrays: Catalyst deactivation or feedstock diffusion controlled? J. Phys. Chem. C 112 (13) (2008) 4892–4896, https://doi.org/10.1021/jp710730x.

[34] A.F.A. Trompeta, Growth and Modification Optimization of 1D Carbon Nanostructures for Advanced Nanomaterial Reinforcement, School of Chemical Engineering, NTUA, Athens, 2021.

[35] H. Almkhelfe, J. Carpena-Núñez, T.C. Back, P.B. Amama, Gaseous product mixture from Fischer-Tropsch synthesis as an efficient carbon feedstock for low temperature CVD growth of carbon nanotube carpets, Nanoscale 8 (27) (2016) 13476–13487, https://doi.org/10.1039/c6nr03679a.

[36] E. Einarsson, Y. Murakami, M. Kadowaki, S. Maruyama, Growth dynamics of vertically aligned single-walled carbon nanotubes from in situ measurements, Carbon 46 (6) (2008) 923–930, https://doi.org/10.1016/j.carbon.2008.02.021.

[37] S.V. Bulyarskiy, G.G. Gusarov, A.V. Lakalin, M.S. Molodenskiy, A.A. Pavlov, R. M. Ryazanov, Vertically aligned carbon nanotube arrays growth modeling at different temperatures and pressures in reactor, Diamond Relat. Mater. 103 (2020) 107665.

[38] K.E. Kim, K.J. Kim, W.S. Jung, S.Y. Bae, J. Park, J. Choi, J. Choo, Investigation on the temperature-dependent growth rate of carbon nanotubes using chemical vapor deposition of ferrocene and acetylene, Chem. Phys. Lett. 401 (4–6) (2005) 459–464, https://doi.org/10.1016/j.cplett.2004.11.113.

[39] O.A. Louchev, T. Laude, Y. Sato, H. Kanda, Diffusion-controlled kinetics of carbon nanotube forest growth by chemical vapor deposition, J. Chem. Phys. 118 (16) (2003) 7622–7634, https://doi.org/10.1063/1.1562195.

[40] V. Jourdain, C. Bichara, Current understanding of the growth of carbon nanotubes in catalytic chemical vapour deposition, Carbon 58 (2013) 2–39, https://doi.org/10.1016/j.carbon.2013.02.046.

[41] C. Ducati, I. Alexandrou, M. Chhowalla, G.A.J. Amaratunga, J. Robertson, Temperature selective growth of carbon nanotubes by chemical vapor deposition, J. Appl. Phys. 92 (6) (2002) 3299–3303, https://doi.org/10.1063/1.1499746.

[42] A. Jorio, R. Saito, Raman spectroscopy for carbon nanotube applications, J. Appl. Phys. 129 (2) (2021) 021102.

[43] S. Musso, S. Porro, M. Rovere, M. Giorcelli, A. Tagliaferro, Fluid dynamic analysis of gas flow in a thermal-CVD system designed for growth of carbon nanotubes, J. Cryst. Growth 310 (2) (2008) 477–483, https://doi.org/10.1016/j.jcrysgro.2007.10.064.

[44] M. Picher, E. Anglaret, V. Jourdain, High temperature activation and deactivation of single-walled carbon nanotube growth investigated by in situ Raman measurements, Diamond Relat. Mater. 19 (5–6) (2010) 581–585, https://doi.org/10.1016/j.diamond.2009.12.003.

[45] X. Feng, K. Liu, X. Xie, R. Zhou, L. Zhang, Q. Li, S. Fan, K. Jiang, Thermal analysis study of the growth kinetics of carbon nanotubes and epitaxial graphene layers on them, J. Phys. Chem. C 113 (22) (2009) 9623–9631, https://doi.org/10.1021/jp901245u.

[46] S. Yasuda, T. Hiraoka, D.N. Futaba, T. Yamada, M. Yumura, K. Hata, Existence and kinetics of graphitic carbonaceous impurities in carbon nanotube forests to assess the absolute purity, Nano Lett. 9 (2) (2009) 769–773, https://doi.org/10.1021/nl803389v.

[47] S. Chaisitsak, J. Nukeaw, A. Tuantranont, Parametric study of atmospheric-pressure single-walled carbon nanotubes growth by ferrocene-ethanol mist CVD, Diamond Relat. Mater. 16 (11) (2007) 1958–1966, https://doi.org/10.1016/j.diamond.2007.09.013.